Simulation of absorption and scattering spectra of crystalline organic nanoparticles with the discrete dipole approximation

Zutterman, Freddy; Champagne, Benoît

Published in:
The Journal of chemical physics

DOI:
10.1063/5.0064930

Publication date:
2021

Document Version
Publisher's PDF, also known as Version of record

The Journal of Chemical Physics

Simulation of absorption and scattering spectra of crystalline organic nanoparticles with the discrete dipole approximation: Effects of crystal shape, crystal size, and refractive index of the medium

Cite as: J. Chem. Phys. **155**, 164703 (2021); https://doi.org/10.1063/5.0064930
Submitted: 28 July 2021 • Accepted: 08 October 2021 • Published Online: 27 October 2021

Freddy Zutterman and Benoît Champagne

The Journal of Chemical Physics ARTICLE scitation.org/journal/jcp

Simulation of absorption and scattering spectra of crystalline organic nanoparticles with the discrete dipole approximation: Effects of crystal shape, crystal size, and refractive index of the medium

Cite as: J. Chem. Phys. 155, 164703 (2021); doi: 10.1063/5.0064930
Submitted: 28 July 2021 • Accepted: 8 October 2021 •
Published Online: 27 October 2021

Freddy Zutterman[a] and Benoît Champagne[b]

AFFILIATIONS

Laboratoire de Chimie Théorique (LCT), Namur Institute of Structured Matter (NISM), University of Namur (UNamur), Rue de Bruxelles, 61, B-5000 Namur, Belgium

[a]Electronic mail: freddy.zutterman@unamur.be
[b]Author to whom correspondence should be addressed: benoit.champagne@unamur.be

ABSTRACT

The effect of the shape (habit) of crystalline organic nanoparticles on their absorption spectra is studied by simulations using the discrete dipole approximation, focusing, in particular, on the vibronic structure of the absorption bands in the spectra. Simulations predict a significant effect that, for sufficiently small particles, can be simply rationalized by the depolarization factor. The crystal size and the refractive index of the medium in which the nanoparticles are embedded are also found to have an effect on the absorption spectra. All factors mentioned are found to influence also the spectra of scattered light. These effects, already broadly documented for metallic nanoparticles, are here demonstrated theoretically for the first time for crystalline organic nanoparticles, providing novel insight into the optical response of such particles. The effects are expected to be displayed by all organic nanoparticles, as long as they have a well-defined crystal structure and are large enough for the optical properties to be understandable using a macroscopic dielectric tensor. The effects demonstrated here should be taken into account when rationalizing differences in absorption spectra of a substance in solution and in nanoparticle form, e.g., in deducing the type of intermolecular packing. The effects are much less pronounced for optically isotropic nanoparticles.

I. INTRODUCTION

Colored organic pigments of many structural families (mainly azo pigments, quinacridones, perylenes, diketopyrrolopyrroles, and phthalocyanines) are used on a large scale in subtractive color systems in applications such as paints, plastics, textile, lacquers, and inks in important industrial areas, e.g., automotive applications, offset printing, and inkjet printing. Synthesis, properties, and applications of organic pigments belonging to these and other families have been extensively reviewed.[1,2]

Subtractive color systems[3] are based on the use of a minimal number of colorants absorbing in different wavelength ranges of the visible part of the electromagnetic spectrum. Typically, and ideally, three different pigments with appropriate absorption spectra can lead to a satisfactory color gamut, i.e., a yellow pigment, a magenta pigment, and a cyan pigment. Ideal absorption spectra for such three-colorant systems have been defined.[3,4] Unfortunately, absorption spectra of commercially available pigments are far from ideal.

As an example, a typical cyan pigment that is used in inkjet printing inks (Pigment Blue 15:3, the commercial form of β copper phthalocyanine) has far too much absorption below 600 nm (Fig. S1 in the supplementary material) and is therefore not an ideal pigment for this application, limiting the color gamut that can be obtained if it is used as the cyan component in a CMYK (cyan, magenta, yellow, and black) ink set. In order to compensate for the far from ideal absorption spectra of commercial CMY pigments, the applications specialist can add other colorants to the formulation, e.g., an orange or green pigment.[4] Alternatively, applications chemists can try to optimize the optical properties of a given component by

modifying some aspect of the structure of the pigment, i.e., by "crystal engineering."[5,6]

Several options are available. An obvious option consists in switching to an organic pigment with another *molecular structure*. Many organic colorants are known, and their absorption spectra have often been published in the chemical or applications literature. In some of the widely used pigment families (e.g., in particular, yellow pigments of the azoacetoacetanilide class), a broad plethora of structural variants are commercially available. The chemist may even try to custom-synthesize pigments with modified molecular structures, being guided by state-of-the-art quantum chemistry tools that allow the prediction of absorption spectra in the solution of organic compounds of dye- or pigment-like molecular complexity,[7–12] including the vibronic structure. Prediction of the vibronic structure of the spectra, determining the width and shape of the absorption band, is essential in applications of dyes and pigments as colorants.

However, organic pigments (contrary to organic dyes) are used as dispersions of nanocrystals or microcrystals in some suitable carrier medium in which they are insoluble. It has been widely demonstrated that the absorption spectrum of a particulate dispersion of a given organic pigment can be very different from the absorption spectrum of a molecular solution of the same substance. Pigment Blue 15:3 provides a particularly striking illustration of this fact (Fig. S1 of the supplementary material). Apart from the fact that the absorption occurs in approximately the same spectral region, the two spectra have essentially nothing in common. Spectacularly different spectra of solutions and dispersions of the same substance are also observed with nanocrystals and aggregates of other substances, e.g., perylenes[13] and carotenoids, in particular, lycopene.[14] While these cases are admittedly extreme, for many other colorants, there is also only a limited correspondence between the spectra of a solution and a dispersion. Spectra may be shifted relative to each other and have a different number of bands, and/or their bands may have different relative intensities.

Consequently, even if the absorption spectrum of the dissolved organic colorant is known or can be theoretically calculated, this may be of little utility when its application in a dispersed solid form is considered. Rational modification of a solid form of an organic colorant with the purpose of improving its absorption spectrum requires knowledge of the reasons why the spectra of the same substance in solution and in dispersed form can be so different.

Intermolecular interactions in the solid state are one well-known reason for these differences. When molecules are densely packed together in a crystal, intermolecular coupling of two different types (Coulomb interactions between transition densities, and charge-transfer interactions) are the main reasons for spectral modifications. Additional factors (e.g., the electrostatic crystal field and molecular distortion in the solid state[15]) may also play a role.

Intermolecular interactions have been broadly investigated, explained, and simulated for dimers,[16–23] aggregates,[24–31] and molecular crystals.[32–39] Besides shifts in the excitation energy, the interactions also modify the vibronic structure of the spectra, sometimes strongly. The preferential orientations of the molecules in crystalline organic materials lead to strong directional dependence of optical properties, as observed, e.g., by the phenomenon of directional dispersion[40–42] in macroscopic crystals and thin films. The preferential orientations of the molecules also lead to preferential growth directions and, therefore, to anisotropic particle shapes.

Many organic pigments may crystallize in several different crystal polymorphs.[43] For example, ten polymorphs of copper phthalocyanine[5] and four polymorphs of quinacridone[44] are known. For some pigments, different crystal polymorphs may even be commercially available. Since intermolecular interactions in the crystal depend on the geometry of the molecular packing, it can be expected that each different crystal polymorph displays different intermolecular interactions and, therefore, a different absorption spectrum. Polymorph-dependent absorption spectra are indeed experimentally observed.[5,45,46] Consequently, the choice of a different polymorph, i.e., a different *crystal structure*, is another option for an applications specialist trying to find a pigment with a suitable absorption spectrum.

Crystal size is yet another structural parameter known to co-determine optical properties of organic pigments and other organic nanoparticles or microparticles.[47–64] Larger particle sizes result in reduced color strength for a pigment and changes in the absorption spectrum. In the applications already mentioned, organic pigments typically have particle sizes ranging from several tens of nanometers to several tens of micrometers. The ideal particle size depends on the application, e.g., too large particle size may lead to too much scattering in applications where transparency is required. Several methods are known by which dispersions of organic pigments with different particle sizes can be produced.[54,59,62,65] The reason why the crystal size has an impact on optical properties is not completely understood, although a variety of hypotheses have been suggested, e.g., in particular, lattice softening,[49,53,56] often without clear experimental or theoretical evidence. In only two[63,64] of these past studies, the contributions of absorption and scattering to the extinction have been separated, and in several cases, the different particle sizes are suspected to be related to different crystal structures.[55,57,58] In at least one case,[63] the particle shape changes concomitantly with the particle size. In several studies,[59,61,63,64] the particle size effect is investigated with simulation methods. However, Mie theory[59,61,64] is not appropriate for pigment particles, which are geometrically and optically anisotropic. In one case,[63] an anisotropic method (the discrete dipole approximation) is used, but the simultaneous change in particle shape is not considered. One of the purposes of the present study consists in theoretically investigating the influence of the particle size alone (i.e., at an identical particle shape and crystal structure) on the absorption and scattering spectra.

However, the main issue investigated here is to what extent variations of the *crystal shape* alone (i.e., maintaining the crystal structure and the crystal size) may be responsible for variations in absorption and scattering spectra of nanocrystalline dispersions of organic colorants and to study the effect of such crystal shape variations by simulation methods. If a significant "crystal shape effect" exists, then this may provide another structural parameter that can be manipulated by an applications scientist in order to achieve more suitable absorption spectra. Indeed, it is known that crystal morphologies can be steered by the use of suitable "crystal growth modifiers" or "tailor-made additives."[66–76]

A literature search reveals a number of studies[77–93] mentioning shape effects on the optical properties of organic dye or pigment particles. However, none of these studies gives a clear-cut view on the impact of the crystal shape alone. In most cases, the different

shapes simultaneously have different sizes, degrees of crystallinity, or crystal structure. In some other cases, the particles with different shapes belong to different molecular species. Often emission spectra are shown, but no absorption spectra or the "absorption" spectra shown have a noticeable contribution of scattering. In some other cases, the particles have rather large sizes (i.e., tens of micrometers) and are therefore somewhat outside the scope of the present study. It is interesting to note that, with few exceptions, these articles are about the use of organic dye or pigment nanoparticles or microparticles for opto-electronic applications. Indeed, this is currently a very active domain of investigation,[94–98] in which structural fine-tuning is necessary to optimize the properties. Consequently, "shape effects" may potentially also be used in this type of application. Organic nanoparticles and aggregates with a bewildering plethora of "nanomorphologies" have been produced, e.g., nanobelts,[99,100] nanowires,[101,102] nanosheets,[103] nanoribbons,[104,105] nanorods,[106,107] and even hollow structures like nanotubes[104,106] or hollow nanoprisms.[108] In most cases, the absorption spectrum of the nanoparticles differs from the spectrum of the same substance in solution, and this difference is usually rationalized as being due to the molecular packing, ignoring possible influences of the particle size or shape. Food pigments, e.g., carotenoids,[90,109–115] are yet another area in which many articles have been published mentioning strong differences between absorption spectra in solution and in aggregate form and between aggregates of various types (e.g., H- vs J-aggregates). In this application area also, the spectral differences are usually attributed to differences in molecular packing, neglecting possible contributions by differences in size and/or shape.

On the basis of such published experimental studies, the question of whether the particle shape alone (i.e., without modification of the crystal structure or particle size) influences the optical properties of organic nanoparticles or not remains largely unanswered. Even more surprisingly, the issue seems to have never been addressed theoretically despite the fact that organic nanoparticles have broad application domains, the fact that tools for simulating the relationship between particle shape and optical response are readily available (Sec. II A), and the fact that such shape (and size) effects have been extremely well documented for other types of substances, i.e., metallic nanoparticles[116–129] and, to a lesser extent, inorganic semiconductor nanoparticles.[130–138] Therefore, the issue is at least of high theoretical interest, and possibly of practical interest also if knowledge gained can be put into practice. It is the purpose of this article to answer this question by using theoretical calculations with simple nanocrystalline model morphologies and a simple model dielectric tensor. Crystal "shape" variations considered in the simulations are variations of the *crystal habit*, i.e., it is assumed that the particles have well-defined crystal facets, but the conclusions should be valid also for more rounded shapes, on the condition that the nanoparticles have a well-defined crystal structure that is constant throughout the particle.

While the study of the effects of the crystal shape on the UV/Vis absorption spectrum of organic nanoparticles is the main purpose of this work, the methods used also allow the exploration of effects of the crystal size and the surrounding medium. Both effects are already well documented in the literature cited about metallic nanoparticles.

A particular focus of the study is on the effect of crystal shape/size and host medium on the *vibronic structure* of absorption spectra. Indeed, it is thanks to their vibronic structure that absorption spectra of organic pigments are broad enough to be suitable in applications, and modifications of the vibronic structure are expected to result in differences in applications properties. This aspect is totally absent in spectra of metallic and inorganic semiconductor nanoparticles.

The simulation methodology used in this study is explained in Secs. II A and II B. All new results obtained, and their interpretation, are presented in Secs. III A–III I. A brief comparison with known behavior of metallic nanoparticles is given in Sec. III J, while Sec. IV presents some general conclusions about the relevance of the newly obtained results.

II. METHODOLOGY

A. The discrete dipole approximation

Many theoretical methods (and computer codes in which they are implemented), e.g., Discrete Dipole Approximation (DDA), finite-difference time domain (FDTD), boundary-element method (BEM), and so on, have been used in the simulation of shape-dependent effects in the absorption spectra of metallic nanoparticles. The relative merits of these approaches have been discussed in several review articles.[139–141] For the work reported here on organic nanocrystals, the discrete dipole approximation,[142,143] implemented in the freely available DDSCAT code,[144] was found to be particularly suitable. The scope and limitations of this approximation have been well investigated,[145–148] and it has been successfully used[121,123,124] in simulations of metallic nanoparticles that, like organic pigment nanoparticles, are strongly absorptive at visible wavelengths.

DDSCAT requires only the particle shape and size and (for an optically anisotropic particle) three orthogonal wavelength-dependent complex refractive indices as input. The three refractive indices are each related to an element of the dielectric tensor ($n^2 = \varepsilon$) of the crystalline substance. In DDSCAT, the dielectric tensor is considered to be diagonal (i.e., the coordinate system for the dielectric tensor needs to be chosen such as to make it diagonal). The orientation of the principal axes of the tensor relative to the crystal shape also needs to be known. Different values of the refractive index of the host medium (e.g., solvent) can also be chosen. The optical response (absorption and scattering) can be averaged over a large number of particle orientations relative to the illuminating plane wave.

It is important to note that, in this study, the crystalline particles are assumed to be large enough for their dielectric/optical properties to be describable by using the dielectric tensor of the bulk substance. On the basis of experience in simulations of the properties of metallic and dielectric nanoparticles,[149–151] this probably limits the validity of the results to nanocrystals with sizes larger than 10 nm. Smaller particles would require other methodologies (e.g., quantum-chemical calculations on large molecular clusters).

B. Model dielectric tensor

The model dielectric tensor is given the following form, with the additional requirement that for the two purely real elements $\varepsilon_{ry} = \varepsilon_{rz}$,

$$\begin{bmatrix} \varepsilon_{rx} + i\varepsilon_{ix} & 0 & 0 \\ 0 & \varepsilon_{ry} & 0 \\ 0 & 0 & \varepsilon_{rz} \end{bmatrix}. \quad (1)$$

A dielectric tensor of this form is strictly valid only for an optically uniaxial crystal, i.e., with crystal symmetries belonging to tetragonal, trigonal, or hexagonal space groups. Organic pigment crystals most often have lower symmetries (i.e., orthorhombic, monoclinic, or triclinic) and their dielectric tensor has a more complicated form.

However, an orthorhombic approximation is a good approximation for lower-symmetry crystals at frequencies in the visible range if there is only one single electronic transition of large oscillator strength (with its associated vibronic structure) in this frequency range.[152,153] In the model used here, it is further assumed that all molecular transition dipole moments are oriented in parallel (i.e., no Davydov splitting, leading to only one complex element) and that the background dielectric is isotropic, leading effectively to a uniaxial model.

If the fundamental properties of this high-oscillator strength "optical" excitation in the crystal are known, the complex element ε_x of the model dielectric tensor can be obtained as a sum over vibronic excitations,

$$\varepsilon_{rx}(\omega) = \varepsilon_\infty + \frac{2N}{\varepsilon_0 \hbar} \sum_j \frac{\mu_{0j}^2 \omega_{0j} \left(\omega_{oj}^2 - \omega^2\right)}{\left(\omega_{0j}^2 - \omega^2\right)^2 + \gamma_{0j}^2 \omega^2}, \tag{2}$$

$$\varepsilon_{ix}(\omega) = \frac{2N}{\varepsilon_0 \hbar} \sum_j \frac{\mu_{0j}^2 \omega_{0j} \gamma_{0j} \omega}{(\omega_{0j}^2 - \omega^2)^2 + \gamma_{0j}^2 \omega^2}. \tag{3}$$

The purely real constant ε_∞ is the "background dielectric" representing the contribution of electronic excitations at higher energies, is considered to be equal to $\varepsilon_{ry/rz}$, and is assumed to be constant over the frequency range of interest; ε_0 is the dielectric permittivity of the vacuum; N is the number of molecules per unit volume in the crystal; $\hbar$ is Planck's constant divided by 2π; ω is the angular frequency of the light; and ω_{0j} and μ_{0j} are the angular resonance frequencies and transition dipole moments for the transitions 0–j responsible for the optical response in the visible frequency range. Since only one electronic excitation is assumed to be present in this frequency range, these transitions 0–j are vibronic excitations within this single electronic excitation. The pure Lorentz oscillator model expressed in Eqs. (2) and (3) is unrealistic, giving too much absorbance far from the resonances. Therefore, the damping factors γ_{0j} were modified by using "Kim" oscillators[154] instead, i.e., they were made frequency-dependent,

$$\gamma_{0j}^{Kim} = \gamma_{0j} \exp\left[-\alpha\left(\frac{\omega - \omega_{0j}}{\gamma_{0j}}\right)^2\right]. \tag{4}$$

The parameter α allows the peak shapes in the spectrum of the imaginary component of the tensor to be modified between approximately Gaussian ($\alpha = 1$) and pure Lorentzian ($\alpha = 0$).

The choice of a constant background dielectric also constitutes a simplification. Some degree of frequency dispersion and anisotropy of this parameter can be expected in reality. However, this simplification does not limit the validity of the conclusions.

Experimental determination of dielectric tensors of organic pigments (e.g., by polarized reflection spectrometry,[155–157] ellipsometry,[158–160] or EELS[161]) is difficult because it is difficult to grow sufficiently large crystals of these substances. Therefore, no attempt was made to accurately reproduce the dielectric tensor of any given specific pigment. However, on the basis of various information (supplementary material), the model dielectric tensor approximately represents quinacridone pigments. Specific parameters used in Eqs. (1)–(4) are given in the supplementary material. The wavelength-dependency of the two components of the complex element ε_x of the model dielectric tensor is shown in Fig. 1.

This model dielectric tensor is not based on any assumptions about the fundamental nature of the electronic transition causing the absorption (i.e., strength of Coulomb coupling, charge-transfer coupling, and solution-to-crystal shift). The absorbing (complex) element ε_x has a main band at 560 nm, a second band at 522 nm, a third band at 490 nm, and a shoulder at about 460 nm. In the "single effective vibrational mode" model used here, these peaks correspond to 0–0, 0–1, 0–2, and 0–3 vibronic transitions.

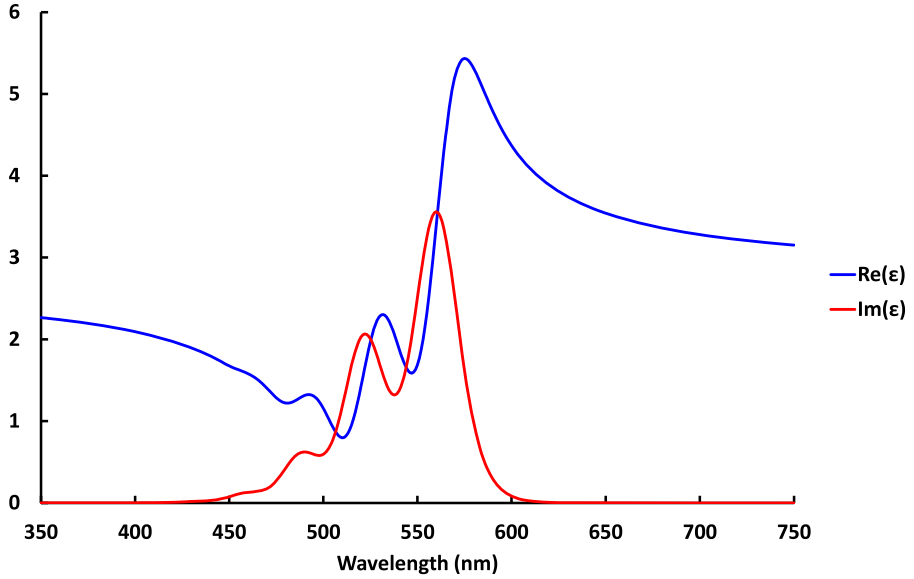

FIG. 1. Real and imaginary components of the complex element ε_x.

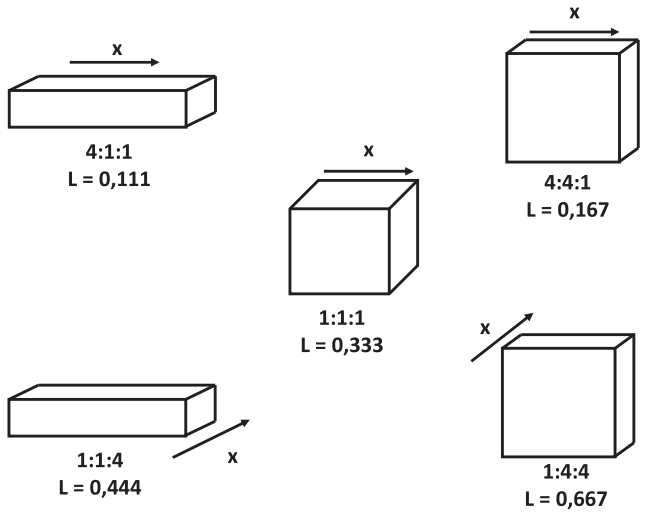

FIG. 2. Model crystal shapes with the orientation of the complex element of the dielectric tensor and approximate depolarization factor L_x.

C. Model nanocrystal shapes and orientation of the dielectric tensor

The calculations were done on very simple model crystal habits, i.e., rectangular solids. While this type of morphology is unlikely to be displayed by common organic pigments, it is the easiest one for demonstrating the effects studied here, without losing relevance and validity of the conclusions. Such particle shapes are very conveniently defined in DDSCAT.

Three different particle shapes were used, i.e., an elongated brick with a square cross section (4:1:1 aspect ratio), a cube, and a square tile (1:4:4 aspect ratio), as illustrated in Fig. 2. The orientations of the principal axes of the dielectric tensor were chosen parallel with the three edges of the particles. For both the 4:1:1 and the 1:4:4 particle shapes, two different orientations of the model dielectric tensor are possible within this definition. The distinction between the two orientations is indicated by specifying the (relative) length of the edge along which the complex (i.e., absorbing) element (x) of the dielectric tensor is aligned as the first element in the aspect ratio. The two different orientations for the elongated brick and the square tile are illustrated in Fig. 2, where the arrows show the orientation of the complex element (x) of the dielectric tensor. In the model pigment considered here, i.e., without Davydov splitting, this orientation corresponds to the orientation of the molecular transition moments (considered to be all parallel to each other). The L values below each shape are the approximate depolarization factors L_x (Sec. III B).

III. RESULTS AND DISCUSSION

A. Effects of the nanocrystal shape on absorption and scattering

Once the shape of the rectangular solid has been defined by selecting the number of dipoles along the three axes (see the supplementary material), DDSCAT requires the particle size to be specified as the effective radius a_{eff} of the particle (i.e., the radius of a sphere of identical volume). In order to be representative of realistic pigment nanoparticles, the effective radius was initially set to 50 nm. Particle dimensions along the three axes are then 203.10 × 50.77 × 50.77, 80.60 × 80.60 × 80.60, and 31.99 × 127.94 × 127.94 nm^3 for the 4:1:1, 1:1:1, and 1:4:4 particle shapes, respectively. Additional calculations, showing the effect of the particle size, were subsequently done with effective radii of 10 and 100 nm (Sec. III F).

The medium in which the nanocrystals are dispersed was initially chosen to have a refractive index of 1.41, which is the refractive index of DEGDEE (diethylene glycol diethyl ether), a solvent often used in pigmented inkjet inks. Additional calculations, showing the effect of the refractive index of the medium, were subsequently done with refractive indices of 1.33 and 1.50 (Sec. III E).

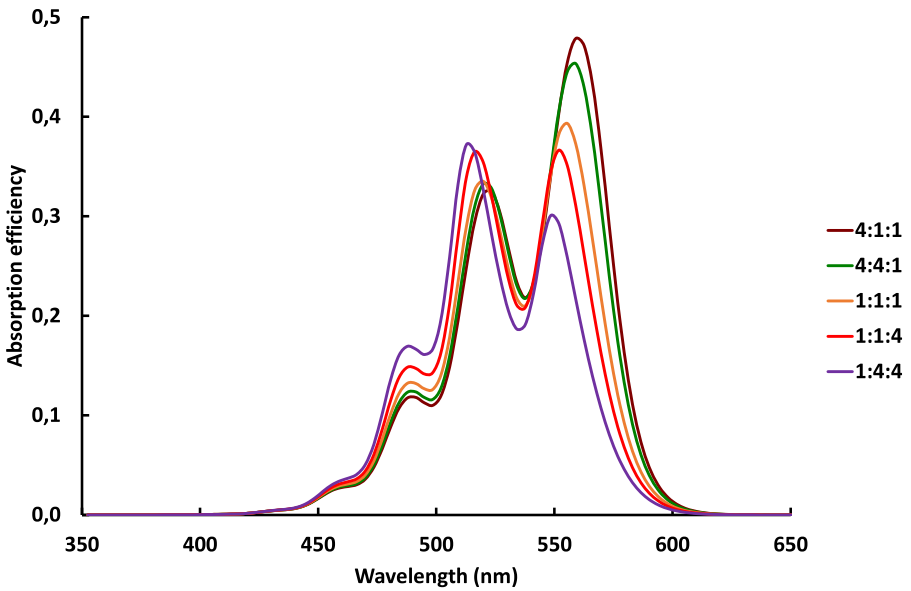

FIG. 3. Orientationally averaged absorption efficiencies as a function of wavelength for particles with different shapes and an effective radius of 50 nm, calculated with DDSCAT.

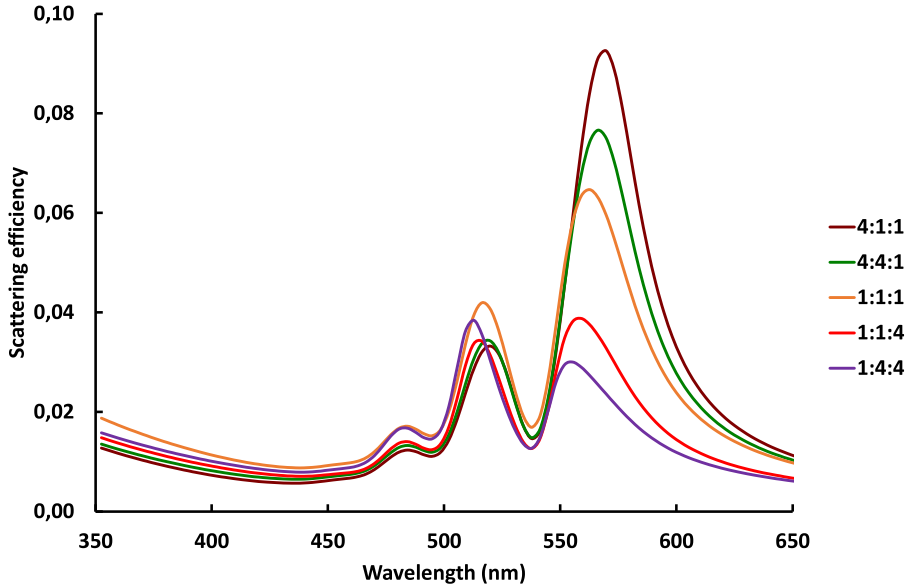

FIG. 4. Orientationally averaged scattering efficiencies as a function of wavelength for particles with different shapes and an effective radius of 50 nm, calculated with DDSCAT.

The optical responses calculated with DDSCAT are the absorption and scattering "efficiencies," i.e., the power dissipated in, or scattered by, the nanoparticle under plane wave incidence divided by the power density of the incident wave on the cross-sectional area. Efficiencies are not directly observable experimentally but can be readily translated into a parameter of practical relevance, i.e., transmittance through a dispersion or pigment layer containing the nanoparticles, which is directly observable (see Sec. III G for more details).

Spectra of the orientationally averaged absorption and scattering efficiencies (Q_{abs} and Q_{sca}) obtained with DDSCAT for the five different particles with an effective radius of 50 nm shown in Fig. 2 are illustrated in Figs. 3 and 4. Wavelengths in this and following figures are the wavelengths in air. All results presented in Sec. III A were obtained by using the dielectric tensor shown in Fig. 1 and DEGDEE as the solvent.

When modifying the particle shape and/or dielectric tensor orientation, a substantial redistribution of intensity over the four vibronic bands is observed. In series 4:1:1–4:4:1–1:1:1–1:1:4–1:4:4, the "0–0" band (at the longest wavelength) progressively loses intensity in favor of the bands at shorter wavelengths, particularly the "0–1" band. Similar redistribution of intensity over the vibronic bands is observed in the spectra of the scattering efficiency (Fig. 4).

For very small particles (effective radius = 10 nm), the intensity transfer toward the vibrational satellites is even more obvious, and the spectral change between the five particles is even smoother, as shown for the absorption efficiency (Fig. 5) and the scattering efficiency (Fig. S2). The two limiting cases were obtained with

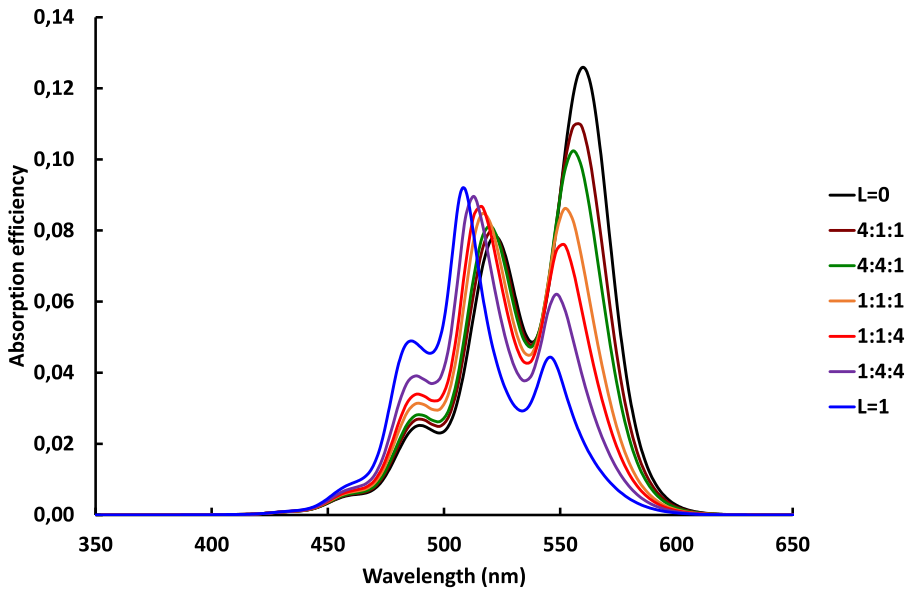

FIG. 5. Orientationally averaged absorption efficiencies as a function of wavelength for particles with different shapes and an effective radius of 10 nm.

Eqs. (5) and (6) (Sec. III B), and the others were obtained with DDSCAT.

B. Interpretation and analysis in the Rayleigh limit

DDSCAT provides results that are accurate within the limits of the discrete dipole approximation for any crystal shape and size. However, the theory of the discrete dipole approximation does not allow for an easy interpretation and explanation of the results. Interpretation is easier in the Rayleigh limit (i.e., particles much smaller than the wavelength) because it was found that the orientationally averaged absorption and scattering efficiencies can then be simply calculated as follows:[117]

$$Q_{abs(avg)}(\lambda_{vac}) = \frac{8\pi r}{9\lambda_{vac}} \sum_k \frac{\varepsilon_{ik}\varepsilon_h^{3/2}}{[L_k\varepsilon_{rk} + (1-L_k)\varepsilon_h]^2 + L_k^2\varepsilon_{ik}^2}, \quad (5)$$

$$Q_{sca(avg)}(\lambda_{vac}) = \frac{128}{81}\left(\frac{\pi r}{\lambda_{vac}}\right)^4 \sum_k \frac{\varepsilon_h^2[(\varepsilon_{rk}-\varepsilon_h)^2 + \varepsilon_{ik}^2]}{[L_k\varepsilon_{rk} + (1-L_k)\varepsilon_h]^2 + L_k^2\varepsilon_{ik}^2}. \quad (6)$$

The k indices refer to the directions x, y, and z. The L factors are geometric depolarization factors, λ_{vac} is the wavelength in a vacuum, and ε_h is the (isotropic) dielectric constant of the host medium in which the particles are embedded (i.e., taken as the DEGDEE solvent in these simulations). The effective radius is represented in the two equations by the symbol r. With the dielectric tensor defined in Sec. II B, the sum in Eq. (5) reduces to one single term (only one "absorbing" axis), but the sum notation is conserved for the sake of consistency.

No exact equations are known for L factors of rectangular solids. However, it was found that satisfactory results are obtained either by using the L factors for ellipsoids[117] with the same relative lengths of their principal axes or even by a very simple equation[162]

$$L_k = \frac{1}{d_k \sum_k \left(\frac{1}{d_k}\right)}. \quad (7)$$

The d_k parameters are the lengths of the particle along the three perpendicular axes. The L values shown in Fig. 2 are depolarization factors for the "absorbing" axis (i.e., L_x), calculated with Eq. (7). The results so obtained are very close to those obtained with DDSCAT for 10 nm particles, as can be judged in Fig. 6 and Fig. S3 for the case of a 1:1:1 particle ($L_x = 1/3$).

In order to explore the limits of Rayleigh theory, the results obtained with DDSCAT and with Eq. (5) are also compared for the 50 nm particle with 1:1:1 shape (Fig. S4 of the supplementary material). For these larger particles, the shape of the spectrum (i.e., relative intensities of the bands) is not correctly reproduced with Eq. (5). Indeed, Eq. (5) produces the same spectral shape for all particle sizes since the particle size is absent in the second part of the equation.

Equations (5) and (6) are strictly valid only in the Rayleigh limit and can only be used if the depolarization factor of the particle is known (at least approximately), so they are useless for crystal habits more complex than the ones used here. However, the merit of Rayleigh theory is that, for both the absorption and scattering spectra, it demonstrates that the intensity transfer over the vibronic bands with changing particle shape is predominantly determined by a very simple parameter, the depolarization factor.

C. Similarity and difference with the effect of exciton coupling

The effect of changes in the crystal habit on the absorption spectrum essentially consists in a modification of the vibronic structure, without substantial changes in the global intensity of the absorption.

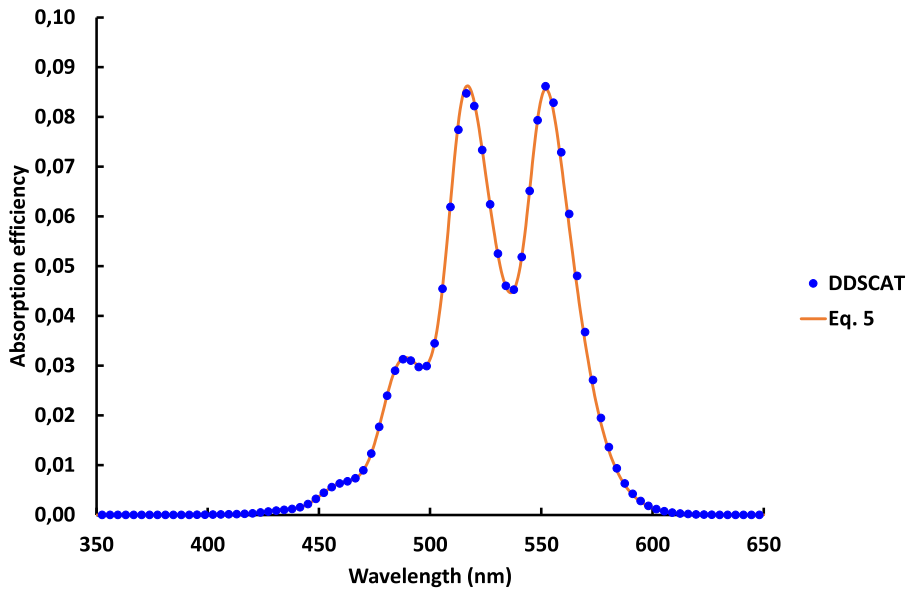

FIG. 6. Orientationally averaged absorption efficiencies as a function of wavelength for the 1:1:1 particle with an effective radius of 10 nm, obtained with DDSCAT and with Eq. (5).

At first sight, the effect is highly reminiscent of the effect of exciton coupling. Indeed, relative to the vibronic structure for a molecule in solution, the vibronic structure of the absorption spectrum of aggregated molecules (dimers, oligomers, aggregates, and crystals) is often distinctly different. "Changes" in the vibronic structure here means redistribution of the intensity over the vibronic bands in the spectrum. The effect of an increasingly higher depolarization factor is like changing from J-aggregation to H-aggregation, i.e., strikingly similar to the effect of an increasingly positive exciton shift.[23,28]

However, it should be stressed that the two phenomena have totally different origins since spectral changes due to exciton coupling have their origin in the intermolecular packing, not the boundaries of the crystal. It can even be imagined that the two mechanisms may have opposite effects, i.e., exciton coupling modifying the spectrum one way (relative to the spectrum of the substance in solution) and the crystal shape moving it the other way.

D. Analogy with directional dispersion in macrocrystals

Changes in the shape of the Q_{abs} spectrum of nanocrystals with varying depolarization factor are strongly related to spectral changes due to "directional dispersion"[40–42] in macroscopic crystals in polarized reflection or transmission spectroscopy.

The normal modes of electromagnetic waves in a macroscopic medium are solutions to the Fresnel equation for refractive indices, which reduces to the following form [Eq. (8)] for a diagonal dielectric tensor, the symbols s_j being the projection of the unit wave vector onto the axes of the dielectric tensor,[163]

$$\begin{aligned}&(n^2-\varepsilon_y)(n^2-\varepsilon_z)\varepsilon_x s_x^2+(n^2-\varepsilon_z)(n^2-\varepsilon_x)\varepsilon_y s_y^2\\&+(n^2-\varepsilon_x)(n^2-\varepsilon_y)\varepsilon_z s_z^2=0.\end{aligned}\tag{8}$$

The two solutions for n^2 give the (squares of the) complex refractive indices of two perpendicularly polarized waves in the medium. For the uniaxial case studied here and for perpendicular incidence, it is easily found that the imaginary part of one of the solutions, i.e., representing the extraordinary wave, is as follows:

$$\mathrm{Im}\left[n_{EX}^2\right]=\frac{\varepsilon_{ix}\varepsilon_\infty^2(1-\sin^2\alpha)}{\left[\varepsilon_{rx}\sin^2\alpha+\varepsilon_\infty(1-\sin^2\alpha)\right]^2+\varepsilon_{ix}^2\sin^4\alpha}.\tag{9}$$

The angle α is the angle between the x dielectric axis and the crystal face (or for perpendicular incidence, $90^\circ-\alpha$ is the angle between the x dielectric axis and the wave vector). The second solution, representing the ordinary wave, is given simply by the background dielectric constant.

Equation (9) has the same structure as Eq. (5) for Q_{abs}, $\sin^2\alpha$ has the same role in the denominator of Eq. (9) as the depolarization factor L_x in Eq. (5), and consequently, both equations produce exactly the same spectral shapes. The close analogy between the two phenomena can be judged by comparing Figs. 5 and 7. Contrary to what is the case in Fig. 5, the additional factor $(1-\sin^2\alpha)$ in the numerator of Eq. (9) causes a gradual reduction in overall intensity with increasing α (the extraordinary wave vanishes for $\alpha=90^\circ$).

As far as the spectral shape is concerned, increasing the depolarization factor in the nanocrystal has exactly the same effect as increasingly tilting the orientation of the "absorbing" (x) element of the dielectric tensor relative to a macroscopic crystal surface.

The effect of directional dispersion in macrocrystals has been explained as being due to the "bulk polarization" at the crystal boundary. Similarly, the effect of the crystal habit in nanocrystals can be ascribed to the overall polarization at the boundaries of the particle.

E. Influence of the refractive index of the host medium

Equation (5) allows convenient simulations for extreme cases of depolarization in the Rayleigh limit. In the case of $L_x=0$ (i.e., a

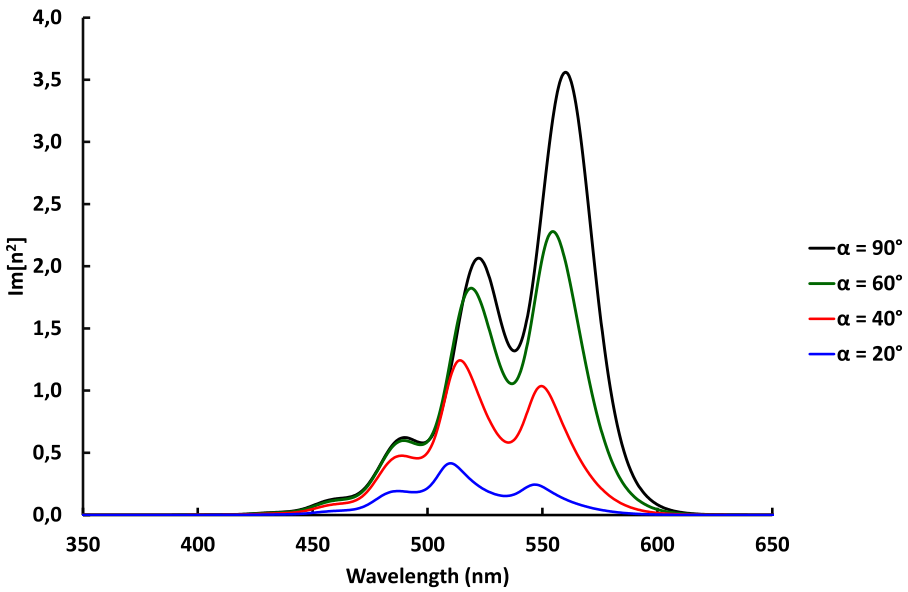

FIG. 7. Solution of Fresnel's equation for refractive indices for the extraordinary wave at perpendicular incidence in a uniaxial macrocrystal, with varying angle between the x direction of the dielectric tensor and the crystal surface (dielectric tensor as in Fig. 1).

very long narrow needle), it reduces to

$$Q_{abs(avg)} = \frac{8\pi r}{9\lambda_{vac}} * \frac{\varepsilon_{ix}}{\sqrt{\varepsilon_h}}. \quad (10)$$

In this case, the shape of the Q_{abs} spectrum is determined only by the shape of the spectrum of the imaginary component of the absorbing element of the dielectric tensor (i.e., ε_{ix}). While the amplitude of the absorption efficiency is modulated by the refractive index of the surrounding medium, the spectral shape is not (assuming that there is no wavelength-dispersion of the refractive index of the medium). For all wavelengths, the absorption decreases homogeneously with increasing refractive index of the medium.

In the case of $L_x = 1$ (i.e., a very flat platelet), Eq. (5) reduces to

$$Q_{abs(avg)} = \frac{8\pi r}{9\lambda_{vac}} * \frac{\varepsilon_{ix}}{\varepsilon_{rx}^2 + \varepsilon_{ix}^2} \varepsilon_h^{3/2}. \quad (11)$$

In this case, the spectral shape is determined by both the real and the imaginary components. It is, in fact, determined by the energy-loss function

$$\mathrm{Im}\left(-\frac{1}{\varepsilon_x}\right) = \frac{\varepsilon_{ix}}{\varepsilon_{rx}^2 + \varepsilon_{ix}^2}. \quad (12)$$

The absorption is predicted to increase with increasing refractive index of the medium, again without modification of the spectral shape.

Another interesting special case is the spherical particle (or, to the approximation used here, a cubic particle). This is the case with $L_x = 1/3$. Equation (5) then becomes

$$Q_{abs(avg)} = \frac{8\pi r}{\lambda_{vac}} * \frac{\varepsilon_{ix}\varepsilon_h^{3/2}}{\varepsilon_{rx}^2 + 4\varepsilon_h^2 + 4\varepsilon_{rx}\varepsilon_h + \varepsilon_{ix}^2}. \quad (13)$$

In this case, the spectrum is determined by both the real and imaginary parts of the dielectric tensor. The refractive index of the host medium has a more complicated effect than in the two limiting cases since it appears in both the numerator and the denominator. A lesser impact is expected, and the spectral shape is predicted to depend on the refractive index of the medium.

Predictions made with Eqs. (10)–(13) about the impact of the refractive index of the host medium were checked by simulations with DDSCAT for the 4:1:1, 1:1:1, and 1:4:4 particles with realistic particle size (50 nm). Three different refractive indices were used (n = 1.33, 1.41, and 1.50), spanning a realistic range for common solvents. The result for the 1:4:4 particle with 50 nm effective radius is shown in Fig. 8, while the results for two other particle shapes can be found in the supplementary material (Figs. S5 and S6). Figure 8 can also be compared with Fig. S7 for 1:4:4: particles of 10 nm. Predictions made for very small particles apparently are indeed valid for the 10 nm particles, but the effect is significantly attenuated for the larger particles.

F. Impact of the particle size

In order to check that the particle shape effect exists also for larger particles, simulations with DDSCAT were performed for the 4:1:1, 1:1:1, and 1:4:4 particles with an effective radius of 100 nm. Both the absorption efficiency and the scattering efficiency increase, as expected. However, the shape of the spectra also changes. The shape effect for the 100 nm particles is shown in Fig. 9. It is considerably less pronounced than for the smaller particles (particularly the 10 nm particles), as can be observed by comparing with Figs. 3 and 5. This is also conveniently illustrated by comparing normalized spectra of the absorption efficiency for a given particle shape and different particle sizes. Increasing the size produces spectral changes that are considerable for the 1:4:4 particles (Fig. 10), moderate for the 1:1:1 particles (Fig. S8), and small for the 4:1:1 particles (Fig. S9). For all three particle shapes, the absorption bands shift slightly toward longer wavelengths with increasing particle size.

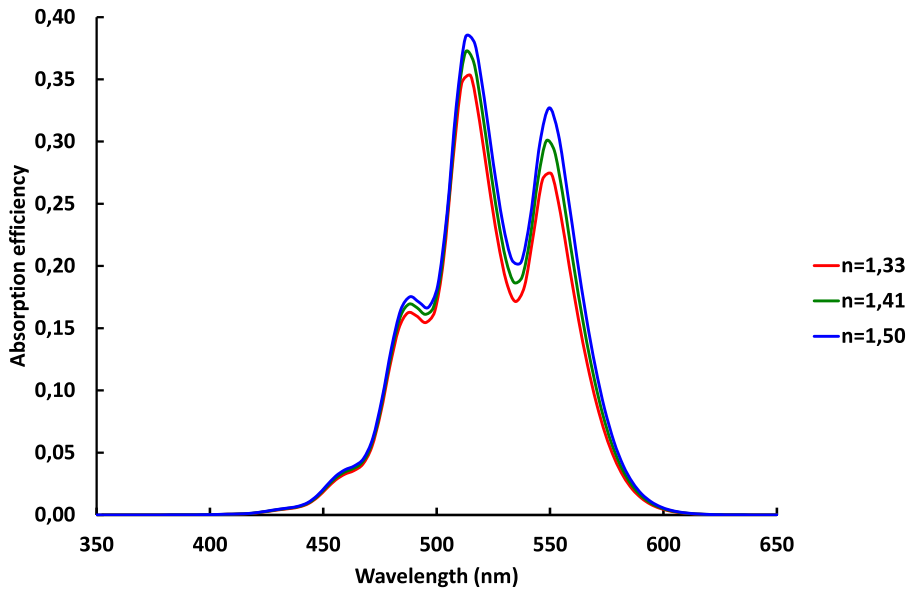

FIG. 8. Orientationally averaged absorption efficiencies as a function of wavelength for the 1:4:4 particle with an effective radius of 50 nm, obtained with DDSCAT with three different refractive indices of the host medium.

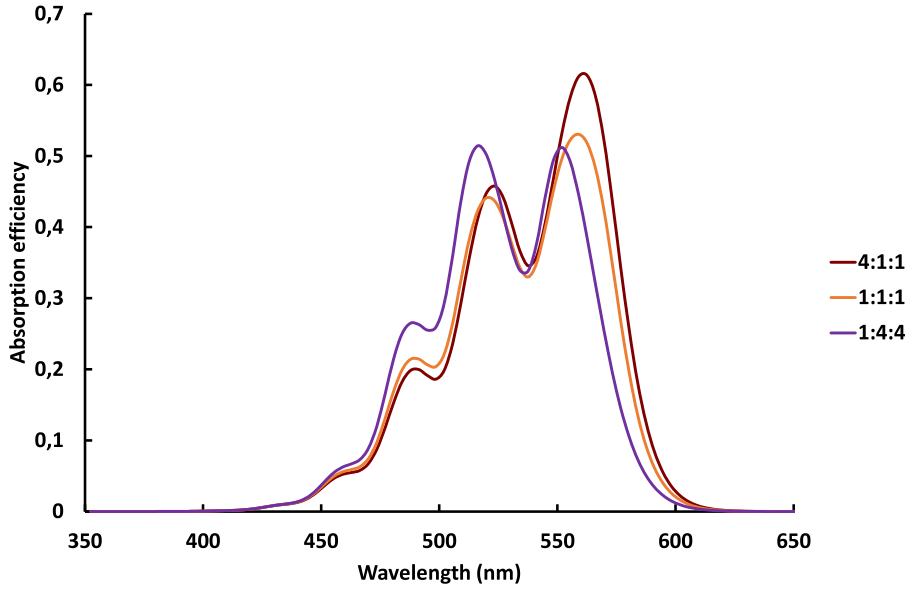

FIG. 9. Orientationally averaged absorption efficiencies as a function of wavelength for particles with different shapes and an effective radius of 100 nm (spectra obtained with DDSCAT).

Fundamental causes for the size-dependency of the response were not clearly identified. However, as for metallic nanoparticles, one likely factor is that the response becomes increasingly less purely dipole-like with increasing size. The comparison between Figs. 3 and 9 also demonstrates that the overall absorption efficiency increases only moderately when the effective particle radius is increased from 50 to 100 nm, even though this represents a fourfold increase in the particle cross section. There is probably a saturation effect, i.e., part of the interior of the larger particles contributes less to the response because of the attenuation inside (a characteristic light penetration depth of 48 nm can be calculated for the maximum of the attenuation constant, i.e., at a wavelength of 556 nm).

G. Observable responses

Absorption and scattering efficiencies are not directly observable but can be readily translated into transmittance through a pigment-containing layer or cuvette. For example, the transmittance T (against a blank of pure solvent) through a cuvette of thickness d containing a pigment of specific gravity ρ at a weight/volume concentration c % is given by Eq. (14), in which $Q_{ext} = Q_{abs} + Q_{sca}$,

$$T = \frac{I_t}{I_0} = e^{-\frac{3cd}{400\rho}\sum_i \frac{f_i Q_{ext}(i)}{r_i}}. \tag{14}$$

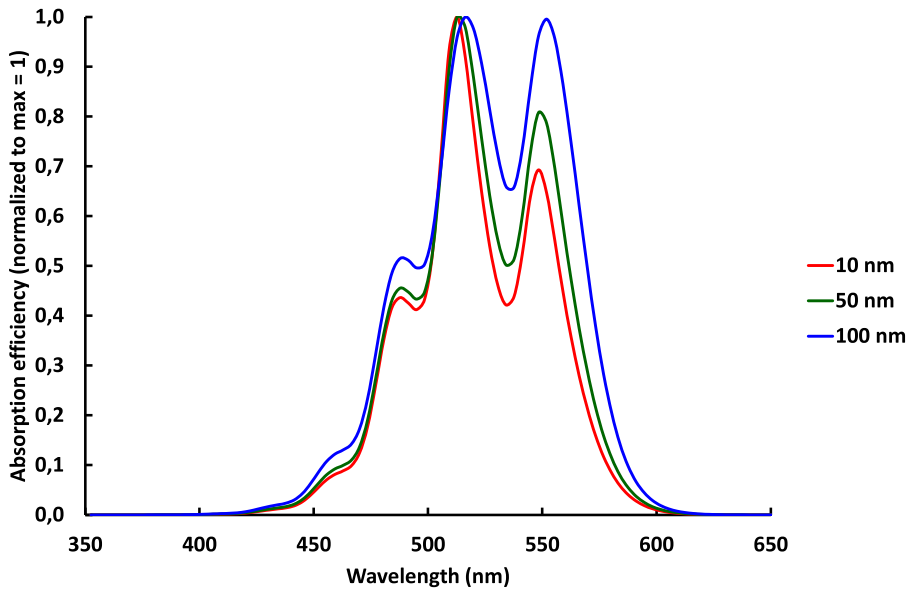

FIG. 10. Orientationally averaged normalized absorption efficiencies as a function of particle size for 1:4:4 particles (spectra obtained with DDSCAT).

Both absorption and scattering contribute to the extinction. In order to see only the contribution of absorption, Q_{ext} can be replaced in Eq. (14) by Q_{abs}.

In a real pigment, different particle sizes are expected to be present. The transmittance is then calculated as a sum over different weight fractions f_i per size class, each with a different extinction efficiency and effective radius. In real pigments, the sum probably also needs to be extended to a distribution of different shapes. Equation (14) was used to calculate the observable transmittance through a 1 cm cuvette containing 0.010% (wt./vol.) of the pigment with a cubic shape and effective radii of 10, 50, and 100 nm. The specific gravity of the pigment crystals was set at 1.5 g/cm^3. The results are shown in Fig. 11. The decreasing transmittance in non-absorbing parts of the spectrum (wings at short and long wavelengths) with increasing particle size (and identical pigment concentration) is due to increasing scattering, as can be demonstrated by leaving out the contribution of the scattering (broken lines, but for the 10 nm particle, the scattering is negligible and the spectrum for pure absorption was not added). Experimentally canceling the contribution of the scattering would necessitate the use of special techniques, e.g., an integrating sphere.[61,63]

The 100 nm pigment is significantly less effective, providing less absorbance for the same pigment loading than the smaller pigments. This is due to the saturation effect mentioned in Sec. III F.

H. Pigments with intrinsically stronger absorption

In order to simulate possible differences between pigment classes absorbing in the same spectral region, e.g., diketopyrrolopyrroles (DPP) vs quinacridones, simulations were also performed with particles exhibiting stronger absorption. To this end, a dielectric tensor was constructed in which the molecular transition dipole moment was increased by 50% (i.e., 2.25× higher oscillator strength) with all other settings remaining equal. The so obtained dielectric tensor element ε_x is shown in Fig. S10. The DDSCAT results for particles with a_{eff} = 50 nm and three different shapes are presented in Fig. 12. The impact of the shape is significantly stronger than for the less strongly absorbing pigment and is even more spectacular for the 10 nm particles (Fig. S11, to be compared with Fig. 5).

I. Optically isotropic particles

A final set of calculations were performed with an isotropic dielectric tensor. To this end, the oscillator strength of the more absorbing molecule (as defined in Sec. III H) was distributed equally over the three axes (keeping all other parameters constant), as might be the case in an amorphous particle in which the molecules are randomly oriented.

The effect of the particle shape is almost negligible in this case, as illustrated in Fig. 13. The comparison with Fig. 12 shows that the spectral shape is similar to the one obtained for an anisotropic particle with a small depolarization factor. The near-absence of a shape effect can be explained by the fact that the oscillator strength along each axis is much smaller (1/3 of the anisotropic case) and the fact that the results for the 1:4:4 and 4:1:1 particles are a sum of small-L and larger-L contributions (resulting in a "medium-L" result like for the 1:1:1 particle).

J. Similarity to shape effects in metal nanoparticles

As explained in the Introduction, all three parameters studied here for highly anisotropic organic nanoparticles (shape, size, and refractive index of the host medium) are already known to influence the optical response of metallic nanoparticles.[116–129] It is therefore of interest to see how these effects compare for both types of nanoparticles. Since the spectra of metallic nanoparticles have no vibronic structure, the comparison is necessarily limited to effects on the absorption band positions only.

Interestingly, the effect of the particle shape on the absorption band positions is much more pronounced for metallic nanoparticles, even though they are optically isotropic. Since metallic

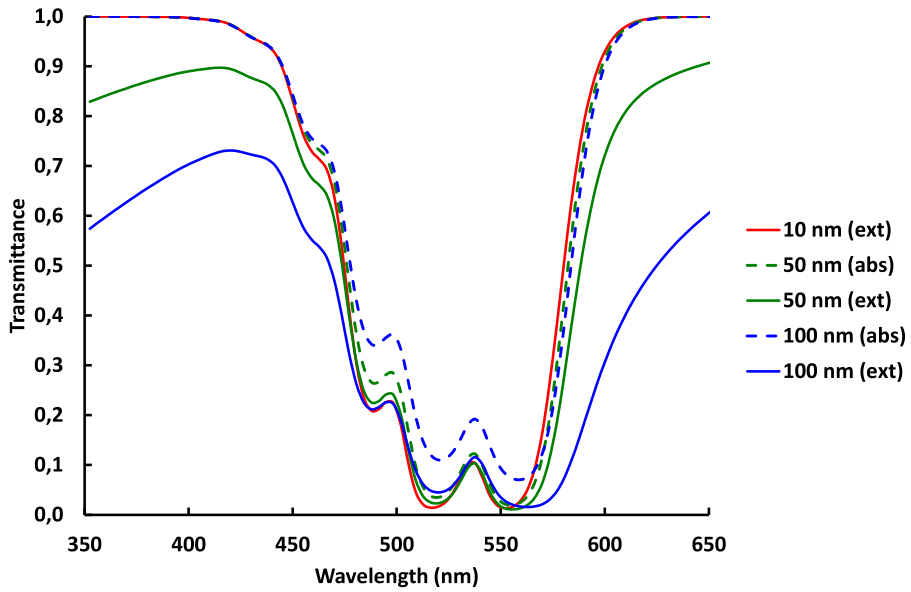

FIG. 11. Transmittance through a 1 cm cuvette containing 0.010% pigment with varying particle size, scattering + absorption (solid lines) and absorption only (broken lines).

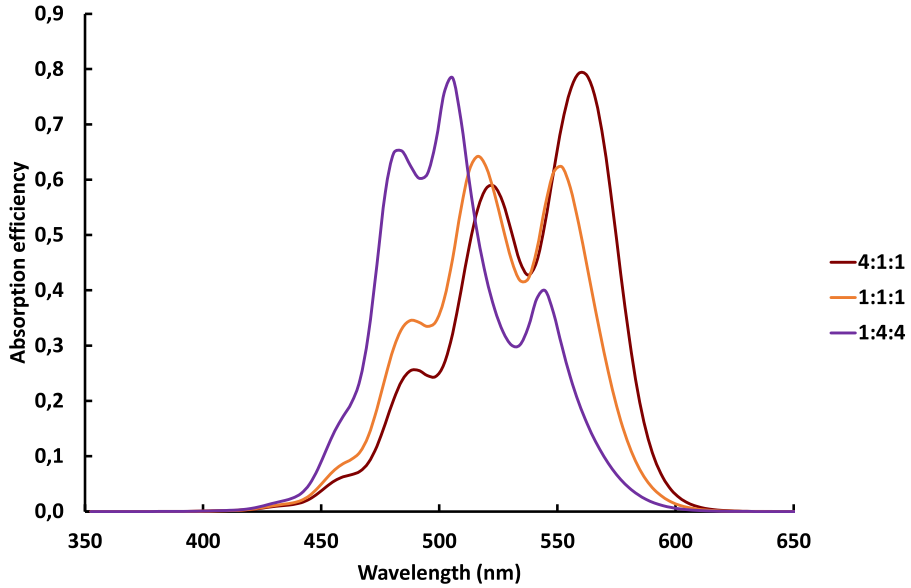

FIG. 12. Orientationally averaged absorption efficiencies as a function of wavelength for particles with different shapes and an effective radius of 50 nm, using the dielectric tensor derived from a 50% larger transition dipole moment.

nanoparticle ellipsoids have three resonances (one along each principal axis), it is difficult to make comparisons with our results. However, the longitudinal resonance in metallic nanoparticle ellipsoids blue-shifts with decreasing aspect ratio.[120] This is similar to the transfer of intensity to the shorter-wavelength vibronic bands with increasing depolarization in our simulations.

For all three particle shapes where size effects were tested (Sec. III F), the absorption bands shift slightly toward longer wavelengths with increasing particle size, and the longer-wavelength vibronic bands gain in (relative) intensity. In metallic nanoparticles, the absorption spectrum moves much more spectacularly to longer wavelengths with increasing particle size.[120,121,123]

Effects of the refractive index of the medium were reported and simulated for the plasmonic resonances of metallic nanoparticles in several studies.[119,123,127,129,164] Here again, the effect is much more pronounced in the metallic species. A similar effect has also been demonstrated for inorganic semiconductor nanoparticles.[165]

The reason for the much more pronounced sensitivity of the metallic nanoparticles to the three factors comes from the fact that the imaginary part of the dielectric function of a metal reaches far more extreme values, and so over a broad frequency range, than for a typical organic pigment or dye crystal.

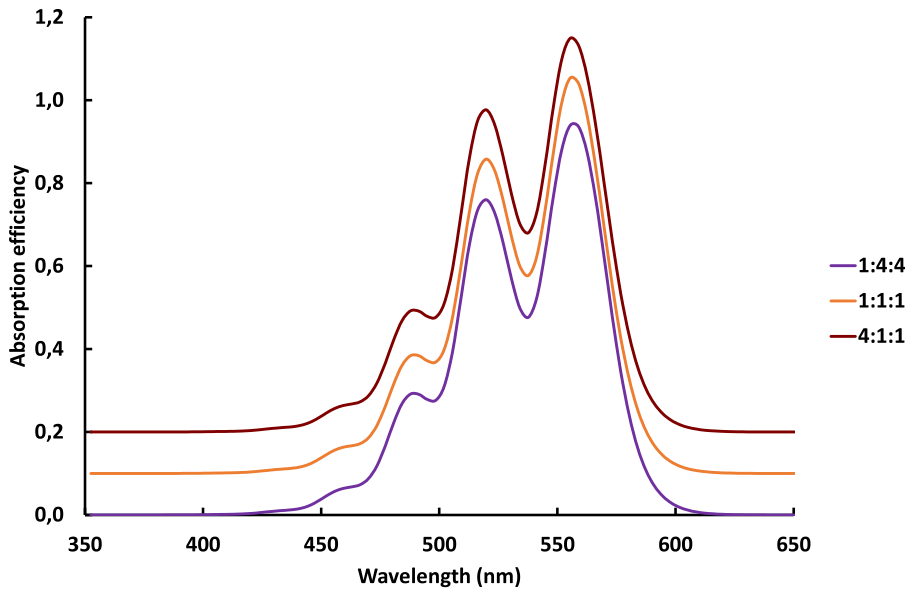

FIG. 13. Orientationally averaged absorption efficiencies as a function of wavelength for particles with different shapes and an effective radius of 50 nm, using an isotropic dielectric tensor derived from the 50% larger transition dipole moment described in Sec. III H (spectrum shifted by 0.1 units for 1:1:1 and by 0.2 units for 1:4:4).

IV. CONCLUSIONS AND OUTLOOK

The pronounced effect of the shape of organic pigment or dye nanoparticles on their absorption (and scattering) spectra, and in particular, on the vibronic structure of the spectra, is here demonstrated for the first time, providing novel insight into the optical response of organic nanoparticles.

Given the fact that the discrete dipole approximation is essentially a method for solving Maxwell's equations for a particle illuminated by a plane wave, the effects found in the simulations are real and should be observable. Further corroboration of this conclusion stems from the fact that the results are confirmed with the analytical equations (5) and (6) in the Rayleigh limit, the fact that the observed effects are similar to those observed with other strongly absorbing particles (i.e., mainly metallic nanoparticles), and the strong analogy with the phenomenon of directional dispersion in large crystals of organic pigments.

The effects should be observable for all organic nanocrystals, i.e., not only for pigments. Unfortunately, unambiguously demonstrating these effects experimentally is a formidable challenge. Indeed, many hard-to-determine parameters need to be unambiguously ascertained experimentally: the crystal structure, the dielectric tensor, the crystal habit, and the crystal size. None of these are easy challenges for organic nanocrystals, and no experimental study is known at present where all criteria are met for unambiguous demonstration of the effects presented here. It is not a surprise that similar issues are encountered when studying the second-order nonlinear optical responses of molecular aggregates of different sizes and shapes.[166] The fact that nanocrystalline organic pigment dispersions are usually stabilized with dispersants further complicates the matter by shielding the pigment from the solvent. The presence of a dispersant around the nanoparticles can, in principle, be taken into account by creating a "mantle" of dipoles with an appropriate refractive index surrounding the particle in DDSCAT.

As a rather general rule, absorption spectra of nanoparticulate dispersions of a substance differ from the absorption spectrum of the same substance in solution, and this is usually explained as being due to the intermolecular couplings in the crystal (Sec. I). Spectral differences between different dispersions of the same substance are also most often explained by differences in molecular packing. The results presented here should invite for some caution in such interpretations. Indeed, spectral changes usually explained by changes in intermolecular coupling can apparently alternatively (or partially) be due to changes in the nanocrystal shape and/or size. Even very large spectral changes, like in the case of β-carotene,[112] can at least, in principle, be explained by nanocrystal habit changes, as illustrated by the results presented in Fig. 12 and Fig. S11 for strongly absorbing particles. Changes in the absorption spectrum due to shape changes are most pronounced when the particles are smaller and the oscillator strength is larger.

By careful experimentation, it would undoubtedly be feasible to demonstrate the shape effect independently of other effects, and such experimental studies are hereby invited and strongly encouraged. The practical usefulness of organic nanocrystal habit modification for fine-tuning absorption spectra also needs to be investigated. The habit of pigment or dye crystals can, in principle, be modified by the use of tailor-made crystal growth modifiers. The simulations, carried out here for very simple model shapes and dielectric tensor orientations, can relatively easily be carried out in DDSCAT for any arbitrary shape and dielectric tensor orientation by specifying the particle shape with the "ANIFRMFIL" keyword and supplying a three-dimensional map of dipole positions. Codes for filling a shape with dipoles can be developed and have already been described.[167] Similarly, simulations are, in principle, feasible for more rounded shapes, such as nanocylinders, nanospheres, and nanotubes, as long as the substance has a well-defined crystal structure (and hence, a well-defined dielectric tensor) throughout the particle. Dielectric tensors of a more complex structure (e.g., with two complex elements due to Davydov splitting or with an anisotropic and/or frequency-dependent background dielectric) can also be easily defined for use in DDSCAT.

Finally, another open question is to what extent the shape effect is still operating in more densely packed ensembles of nanoparticles (e.g., a film deposited on a substrate). All results presented here are valid only for isolated particles, unperturbed by the electromagnetic field induced in neighboring particles. At small inter-particle distances, it can be expected that inter-particle interactions, analogous to exciton interactions between molecules, would further perturb the absorption spectra, as has already been demonstrated for metallic nanoparticles.[168–170] Such interactions can be studied, e.g., with DDSCAT for particle pairs, while larger ensembles of particles can be studied with dedicated methods.[171–173]

SUPPLEMENTARY MATERIAL

See the supplementary material for parameters of the model dielectric tensor, parameters used in DDSCAT, and results of additional supporting and illustrative simulations.

ACKNOWLEDGMENTS

The authors thank Dr. Eng. Thomas Wriedt and Dr. Eng. Roman Schuh of Leibniz-IWT for expert advice and setting up the DDSCAT procedures. Financial support from IWT-Vlaanderen and Agfa in the early stages of this research is gratefully acknowledged.

AUTHOR DECLARATIONS

Conflict of Interest

There are no conflicts to declare.

DATA AVAILABILITY

The data that support the findings of this study are available from the corresponding author upon reasonable request.

REFERENCES

[1] W. Herbst and K. Hunger, *Industrial Organic Pigments: Production, Properties, Applications*, 3rd ed. (Wiley, 2004).
[2] *High Performance Pigments*, 2nd ed., edited by E. B. Faulkner and R. J. Schwartz (Wiley, 2009).
[3] R. W. G. Hunt, *The Reproduction of Colour*, 6th ed. (Wiley, 2004).
[4] Y. Chen, R. S. Berns, and L. A. Taplin, in *12th Color and Imaging Conference Final Program and Proceedings* (The Society for Imaging Science and Technology, 2004), pp. 163–169.
[5] P. Erk, H. Hengelsberg, M. F. Haddow, and R. van Gelder, CrystEngComm **6**, 474–483 (2004).

[6]G. R. Desiraju, Angew. Chem., Int. Ed. **46**, 8342–8356 (2007).
[7]C. Adamo and D. Jacquemin, Chem. Soc. Rev. **42**, 845–856 (2013).
[8]V. Barone, M. Biczysko, J. Bloino, L. Carta, and A. Pedone, Comput. Theor. Chem. **1037**, 35–48 (2014).
[9]B. Champagne, V. Liégeois, and F. Zutterman, Photochem. Photobiol. Sci. **14**, 444–456 (2015).
[10]F. Santoro and D. Jacquemin, Wiley Interdiscip. Rev.: Comput. Mol. Sci. **6**, 460–486 (2016).
[11]F. Zutterman, O. Louant, G. Mercier, T. Leyssens, and B. Champagne, J. Phys. Chem. A **122**, 5370–5374 (2018).
[12]R. Berraud-Pache, F. Neese, G. Bistoni, and R. Izsák, J. Phys. Chem. Lett. **10**, 4822–4828 (2019).
[13]K. Balakrishnan, A. Datar, T. Naddo, J. Huang, R. Oitker, M. Yen, J. Zhao, and L. Zang, J. Am. Chem. Soc. **128**, 7390–7398 (2006).
[14]J. Hempel, C. N. Schädle, S. Leptihn, R. Carle, and R. M. Schweiggert, J. Photochem. Photobiol., A **317**, 161–174 (2016).
[15]W. Li, Q. Peng, H. Ma, J. Wen, J. Ma, L. A. Peteanu, and Z. Shuai, Chem. Mater. **29**, 2513–2520 (2017).
[16]A. Witkowski and W. Moffitt, J. Chem. Phys. **33**, 872–875 (1960).
[17]R. E. Merrifield, Radiat. Res. **20**, 154–158 (1963).
[18]D. Beljonne, J. Cornil, R. Silbey, P. Millié, and J. L. Brédas, J. Chem. Phys. **112**, 4749–4758 (2000).
[19]A. Myers Kelley, J. Chem. Phys. **119**, 3320–3331 (2003).
[20]I. A. Howard, F. Zutterman, G. Deroover, D. Lamoen, and C. Van Alsenoy, J. Phys. Chem. B **108**, 19155–19162 (2004).
[21]A. Eisfeld, L. Braun, W. T. Strunz, J. S. Briggs, J. Beck, and V. Engel, J. Chem. Phys. **122**, 134103 (2005).
[22]M. Andrzejak and P. Petelenz, Chem. Phys. **335**, 155–163 (2007).
[23]J. Guthmüller, F. Zutterman, and B. Champagne, J. Chem. Phys. **131**, 154302 (2009).
[24]M. Kasha, Radiat. Res. **20**, 55–70 (1963).
[25]H. DeVoe, J. Chem. Phys. **41**, 393–400 (1964); **43**, 3199-3208 (1965).
[26]K. Norland, A. Ames, and T. Taylor, Photogr. Sci. Eng. **14**, 295–307 (1970).
[27]G. D. Scholes and G. Rumbles, Nat. Mater. **5**, 683–696 (2006).
[28]A. Eisfeld and J. S. Briggs, Chem. Phys. **324**, 376–384 (2006).
[29]F. C. Spano, Acc. Chem. Res. **43**, 429–439 (2010).
[30]N. J. Hestand and F. C. Spano, Chem. Rev. **118**, 7069–7163 (2018).
[31]D. Bialas, E. Kirchner, M. I. S. Röhr, and F. Würthner, J. Am. Chem. Soc. **143**, 4500–4518 (2021).
[32]A. S. Davydov, *Theory of Molecular Excitons* (Plenum, New York, 1971).
[33]M. R. Philpott, J. Chem. Phys. **52**, 5842–5850 (1970).
[34]D. L. Mills and E. Burstein, Rep. Prog. Phys. **37**, 817–926 (1974).
[35]I. Vragovic and R. Scholz, Phys. Rev. B **68**, 155202 (2003).
[36]J. Knoester and V. M. Agranovich, Thin Films Nanostruct. **31**, 1–96 (2003).
[37]Z. Zhao and F. C. Spano, J. Chem. Phys. **122**, 114701 (2005).
[38]A. Stradomska and P. Petelenz, Acta Phys. Pol., A **112**, S161–S170 (2007).
[39]J. Gierschner, J. Shi, B. Milián-Medina, D. Roca-Sanjuán, S. Varghese, and S. Park, Adv. Opt. Mater. **9**, 2002251 (2021).
[40]H. J. Hesse, W. Fuhs, G. Weiser, and L. von Szentpaly, Phys. Status Solidi B **76**, 817–826 (1976).
[41]S. Möller and G. Weiser, Synth. Met. **122**, 41–43 (2001).
[42]G. Weiser, *Photophysics of Molecular Materials* (Wiley, 2006), pp. 429–496.
[43]J. Bernstein, *Polymorphism in Molecular Crystals* (Oxford University Press, Oxford, 2002).
[44]E. F. Paulus, F. J. J. Leusen, and M. U. Schmidt, CrystEngComm **9**, 131–143 (2007).
[45]R. Sappok, J. Oil Colour Chem. Assoc. **61**, 299–308 (1978).
[46]D. Horn and B. Honigmann, in *FATIPEC Congress* (Federation of Associations of Technicians for Industry of Paints in European Countries, 1974), Vol. 12, pp. 181–189.
[47]P. Hauser, M. Herrmann, and B. Honigmann, Farbe Lack **76**, 545–550 (1970).
[48]P. Hauser and B. Honigmann, Farbe Lack **77**, 1097–1106 (1971).
[49]H. Kasai, H. Kamatani, S. Okada, H. Oikawa, H. Matsuda, and H. Nakanishi, Jpn. J. Appl. Phys., Part 2 **35**, L221–L223 (1996).
[50]H.-B. Fu, X.-H. Ji, X.-H. Zhang, S.-K. Wu, and J.-N. Yao, J. Colloid Interface Sci. **220**, 177–180 (1999).
[51]H.-B. Fu, Y.-Q. Wang, and J.-N. Yao, Chem. Phys. Lett. **322**, 327–332 (2000).
[52]H.-B. Fu and J.-N. Yao, J. Am. Chem. Soc. **123**, 1434–1439 (2001).
[53]R. Xie, H. Fu, X. Ji, and J. Yao, J. Photochem. Photobiol., A **147**, 31–37 (2002).
[54]H. Oikawa, H. Kasai, and H. Nakanishi, ACS Symp. Ser. **798**, 158–168 (2001).
[55]T. Sugiyama, T. Asahi, H. Takeuchi, and H. Masuhara, Jpn. J. Appl. Phys., Part 1 **45**, 384–388 (2006).
[56]A. Patra, N. Hebalkar, B. Sreedhar, M. Sarkar, A. Samanta, and T. P. Radhakrishnan, Small **2**, 650–659 (2006).
[57]H.-G. Jeon, T. Sugiyama, H. Masuhara, and T. Asahi, J. Phys. Chem. C **111**, 14658–14663 (2007).
[58]K. Sue, T. Usami, K. Arai, H. Kasai, H. Nakanishi, and T. Hiaki, Dyes Pigm. **76**, 632–635 (2008).
[59]R. Yasukuni, T. Hironaka, and T. Asahi, Jpn. J. Appl. Phys., Part 1 **49**, 06GJ04 (2010).
[60]R. Yasukuni, M. Sliwa, J. Hofkens, F. C. De Schryver, A. Herrmann, K. Müllen, and T. Asahi, Jpn. J. Appl. Phys., Part 1 **48**, 065002 (2009).
[61]H. Ishino, S. V. Nair, K. Nakagawa, T. Kobayashi, and E. Tokunaga, Appl. Phys. Lett. **99**, 053304 (2011).
[62]A. Y. Utekhina and G. B. Sergeev, Russ. Chem. Rev. **80**, 219–233 (2011).
[63]Y. Numata, S. V. Nair, K. Nakagawa, H. Ishino, T. Kobayashi, and E. Tokunaga, Chem. Phys. Lett. **601**, 128–133 (2014).
[64]J. Gierschner, L. Lüer, B. Milián-Medina, D. Oelkrug, and H.-J. Egelhaaf, J. Phys. Chem. Lett. **4**, 2686–2697 (2013).
[65]R. Li, W. Hu, Y. Liu, and D. Zhu, Acc. Chem. Res. **43**, 529–540 (2010).
[66]Z. Berkovitch-Yellin, J. van Mil, L. Addadi, M. Idelson, M. Lahav, and L. Leiserowitz, J. Am. Chem. Soc. **107**, 3111–3122 (1985).
[67]L. Addadi, Z. Berkovitch-Yellin, I. Weissbuch, J. van Mil, L. J. W. Shimon, M. Lahav, and L. Leiserowitz, Angew. Chem. **97**, 476–496 (1985).
[68]G. Clydesdale, K. J. Roberts, and R. Docherty, J. Cryst. Growth **135**, 331–340 (1994).
[69]G. Clydesdale, K. J. Roberts, K. Lewtas, and R. Docherty, J. Cryst. Growth **141**, 443–450 (1994).
[70]B. D. Chen, J. Garside, R. J. Davey, S. J. Maginn, and M. Matsuoka, J. Phys. Chem. **98**, 3215–3221 (1994).
[71]O.-P. Kwon S.-J. Kwon, M. Jazbinsek, A. Choubey, P. A. Losio, V. Gramlich, and P. Günter, Cryst. Growth Des. **6**, 2327–2332 (2006).
[72]L. Kang, H. Fu, X. Cao, Q. Shi, and J. Yao, J. Am. Chem. Soc. **133**, 1895–1901 (2011).
[73]S.-H. Lee, G.-H. Lee, K.-H. Lee, M. Jazbinsek, B. J. Kang, F. Rotermund, and O.-P. Kwon, Cryst. Growth Des. **16**, 3555–3561 (2016).
[74]K. N. Olafson, R. Li, B. G. Alamani, and J. D. Rimer, Chem. Mater. **28**, 8453–8465 (2016).
[75]Y. Park, J. Y. Koo, and H. C. Choi, Cryst. Growth Des. **18**, 7239–7243 (2018).
[76]P. L. Kaskiewicz, I. Rosbottom, R. B. Hammond, N. J. Warren, C. Morton, P. J. Dowding, N. George, and K. J. Roberts, Cryst. Growth Des. **21**, 1946–1958 (2021).
[77]B. Felder, Helv. Chim. Acta **51**, 1224–1234 (1968).
[78]P. Hauser, D. Horn, and R. Sappok, in *FATIPEC Congress* (Federation of Associations of Technicians for Industry of Paints in European Countries, 1974), Vol. 12, pp. 191–197.
[79]S. Li, L. He, F. Xiong, Y. Li, and G. Yang, J. Phys. Chem. B **108**, 10887–10892 (2004).
[80]A. J. Gesquiere, T. Uwada, T. Asahi, H. Masuhara, and P. F. Barbara, Nano Lett. **5**, 1321–1325 (2005).
[81]X. Zhang, X. Zhang, W. Shi, X. Meng, C. Lee, and S. Lee, J. Phys. Chem. B **109**, 18777–18780 (2005).
[82]F. Bertorelle, F. Rodrigues, and S. Fery-Forgues, Langmuir **22**, 8523–8531 (2006).
[83]Z. Tian, Y. Zhang, Y. Zhang, A. Peng, Y. Ma, Y. Chen, W. Yang, Y. Tang, and J. Yao, J. Nanopart. Res. **8**, 65–77 (2006).

[84]Y. S. Zhao, W. Yang, and J. Yao, Phys. Chem. Chem. Phys. **8**, 3300–3303 (2006).
[85]X. Zhang, C. Dong, J. A. Zapien, S. Ismathullakhan, Z. Kang, J. Jie, X. Zhang, J. C. Chang, C.-S. Lee, and S.-T. Lee, Angew. Chem., Int. Ed. **48**, 9121–9123 (2009).
[86]L. Huang, Q. Liao, Q. Shi, H. Fu, J. Ma, and J. Yao, J. Mater. Chem. **20**, 159–166 (2010).
[87]E. H. Cho, M. S. Kim, D. H. Park, H. Jung, J. Bang, J. Kim, and J. Joo, Adv. Funct. Mater. **21**, 3056–3063 (2011).
[88]D. H. Park, S. G. Jo, Y. K. Hong, C. Cui, H. Lee, D. J. Ahn, J. Kim, and J. Joo, J. Mater. Chem. **21**, 8002–8007 (2011).
[89]X. Zhang, C. Zhao, J. Lv, C. Dong, X. Ou, X. Zhang, and S.-t. Lee, Cryst. Growth Des. **11**, 3677–3680 (2011).
[90]C. Wang, C. J. Berg, C.-C. Hsu, B. A. Merrill, and M. J. Tauber, J. Phys. Chem. B **116**, 10617–10630 (2012).
[91]C. Spies, A.-M. Huynh, V. Huch, and G. Jung, J. Phys. Chem. C **117**, 18163–18169 (2013).
[92]D. Das, G. P. Sahoo, P. Mazumdar, A. Maity, D. Chattopadhyay, G. Salgado-Morán, and A. Misra, J. Mol. Liq. **206**, 47–55 (2015).
[93]C. W. Leishman and J. L. McHale, J. Phys. Chem. C **120**, 15496–15508 (2016).
[94]Y. S. Zhao, H. Fu, A. Peng, Y. Ma, D. Xiao, and J. Yao, Adv. Mater. **20**, 2859–2876 (2008).
[95]A. Patra, Ch. G. Chandaluri, and T. P. Radhakrishnan, Nanoscale **4**, 343–359 (2012).
[96]O. Ostroverkhova, Chem. Rev. **116**, 13279–13412 (2016).
[97]M. Gsänger, D. Bialas, L. Huang, M. Stolte, and F. Würthner, Adv. Mater. **28**, 3615–3645 (2016).
[98]C. Wang, H. Dong, L. Jiang, and W. Hu, Chem. Soc. Rev. **47**, 422–500 (2018).
[99]K. Balakrishnan, A. Datar, R. Oitker, H. Chen, J. Zuo, and L. Zang, J. Am. Chem. Soc. **127**, 10496–40497 (2005).
[100]X. Cao, Y. Wu, H. Fu, and J. Yao, J. Phys. Chem. Lett. **2**, 2163–2167 (2011).
[101]A. L. Briseno, S. C. B. Mannsfeld, C. Reese, J. M. Hancock, Y. Xiong, S. A. Jenekhe, Z. Bao, and Y. Xia, Nano Lett. **7**, 2847–2853 (2007).
[102]J. Wang, Y. Zhao, J. Zhang, J. Zhang, B. Yang, Y. Wang, D. Zhang, H. You, and D. Ma, J. Phys. Chem. C **111**, 9177–9183 (2007).
[103]Y. Lei, Q. Liao, H. Fu, and J. Yao, J. Phys. Chem. C **113**, 10038–10043 (2009).
[104]X. Zhang, X. Zhang, K. Zou, C.-S. Lee, and S.-T. Lee, J. Am. Chem. Soc. **129**, 3527–3532 (2007).
[105]X. Zhang, G. Yuan, Q. Li, B. Wang, X. Zhang, R. Zhang, J. C. Chang, C.-s. Lee, and S.-t. Lee, Chem. Mater. **20**, 6945–6950 (2008).
[106]Y. S. Zhao, J. Xu, A. Peng, H. Fu, Y. Ma, L. Jiang, and J. Yao, Angew. Chem., Int. Ed. **47**, 7301–7305 (2008).
[107]R. Kihara, S. Imada, T. Kawai, and T. Asahi, Appl. Surf. Sci. **478**, 532–538 (2019).
[108]J.-S. Hu, Y.-G. Guo, H.-P. Liang, L.-J. Wan, and L. Jiang, J. Am. Chem. Soc. **127**, 17090–17095 (2005).
[109]I. Inamura, M. Isshiki, and T. Araki, Bull. Chem. Soc. Jpn. **62**, 1671–1673 (1989).
[110]Y. Mori, K. Yamano, and H. Hashimoto, Chem. Phys. Lett. **254**, 84–88 (1996).
[111]H. Auweter, H. Haberkorn, W. Heckmann, D. Horn, E. Lüddecke, J. Rieger, and H. Weiss, Angew. Chem., Int. Ed. **38**, 2188–2191 (1999).
[112]D. Horn and J. Rieger, Angew. Chem., Int. Ed. **40**, 4330–4361 (2001).
[113]F. C. Spano, J. Am. Chem. Soc. **131**, 4267–4278 (2009).
[114]P. Adamkiewicz, A. Sujak, and W. I. Gruszecki, J. Mol. Struct. **1046**, 44–51 (2013).
[115]J. Dong, D. Zhang, X.-Y. Wang, and P. Wang, Chem. Phys. Lett. **701**, 52–57 (2018).
[116]G. Mie, Ann. Phys. **330**, 377–445 (1908).
[117]R. Gans, Ann. Phys. **342**, 881–900 (1912).
[118]C. A. Foss, Jr., G. L. Hornyak, J. A. Stockert, and C. R. Martin, J. Phys. Chem. **98**, 2963–2971 (1994).
[119]S. Link, M. B. Mohamed, and M. A. El-Sayed, J. Phys. Chem. B **103**, 3073–3077 (1999).
[120]S. Link and M. A. El-Sayed, J. Phys. Chem. B **103**, 8410–8426 (1999).
[121]T. Jensen, L. Kelly, A. Lazarides, and G. C. Schatz, J. Cluster Sci. **10**, 295–317 (1999).
[122]J. J. Mock, M. Barbic, D. R. Smith, D. A. Schultz, and S. Schultz, J. Chem. Phys. **116**, 6755–6759 (2002).
[123]K. L. Kelly, E. Coronado, L. L. Zhao, and G. C. Schatz, J. Phys. Chem. B **107**, 668–677 (2003).
[124]M. M. Miller and A. A. Lazarides, J. Phys. Chem. B **109**, 21556–21565 (2005).
[125]N. G. Khlebtsov, L. A. Trachuk, and A. G. Mel'nikov, Opt. Spectrosc. **98**, 77 (2005).
[126]C. Noguez, J. Phys. Chem. C **111**, 3806–3819 (2007).
[127]I. Pastoriza-Santos, A. Sánchez-Iglesias, F. J. García de Abajo, and L. M. Liz-Marzán, Adv. Funct. Mater. **17**, 1443–1450 (2007).
[128]V. Myroshnychenko, J. Rodríguez-Fernández, I. Pastoriza-Santos, A. M. Funston, C. Novo, P. Mulvaney, L. M. Liz-Marzán, and F. J. García de Abajo, Chem. Soc. Rev. **37**, 1792–1805 (2008).
[129]H. Chen, X. Kou, Z. Yang, W. Ni, and J. Wang, Langmuir **24**, 5233–5237 (2008).
[130]C. Burda, X. Chen, R. Narayanan, and M. A. El-Sayed, Chem. Rev. **105**, 1025–1102 (2005).
[131]C. Lizandara-Pueyo, S. Siroky, M. R. Wagner, A. Hoffmann, J. S. Reparaz, M. Lehmann, and S. Polarz, Adv. Funct. Mater. **21**, 295–304 (2011).
[132]G. Garcia, R. Buonsanti, E. L. Runnerstrom, R. J. Mendelsberg, A. Llordes, A. Anders, T. J. Richardson, and D. J. Milliron, Nano Lett. **11**, 4415–4420 (2011).
[133]S.-W. Hsu, K. On, and A. R. Tao, J. Am. Chem. Soc. **133**, 19072–19075 (2011).
[134]M. Liu, X. Xue, C. Ghosh, X. Liu, Y. Liu, E. P. Furlani, M. T. Swihart, and P. N. Prasad, Chem. Mater. **27**, 2584–2590 (2015).
[135]J. Kim, A. Agrawal, F. Krieg, A. Bergerud, and D. J. Milliron, Nano Lett. **16**, 3879–3884 (2016).
[136]R. Lesyuk, E. Klein, I. Yaremchuk, and C. Klinke, Nanoscale **10**, 20640–20651 (2018).
[137]R. M. Córdova-Castro, M. Casavola, M. van Schilfgaarde, A. V. Krasavin, M. A. Green, D. Richards, and A. V. Zayats, ACS Nano **13**, 6550–6560 (2019).
[138]W. Xu, H. Liu, D. Zhou, X. Chen, N. Ding, H. Song, and H. Ågren, Nano Today **33**, 100892 (2020).
[139]T. Wriedt, Part. Part. Syst. Charact. **15**, 67–74 (1998).
[140]T. Wriedt, J. Quant. Spectrosc. Radiat. Transfer **110**, 833–843 (2009).
[141]F. M. Kahnert, J. Quant. Spectrosc. Radiat. Transfer **79–80**, 775–824 (2003).
[142]E. M. Purcell and C. R. Pennypacker, Astrophys. J. **186**, 705–714 (1973).
[143]M. A. Yurkin and A. G. Hoekstra, J. Quant. Spectrosc. Radiat. Transfer **106**, 558–589 (2007).
[144]B. T. Draine and P. J. Flatau, J. Opt. Soc. Am. A **11**, 1491–1499 (1994).
[145]B. T. Draine and J. Goodman, Astrophys. J. **405**, 685–697 (1993).
[146]A. Rahmani, P. C. Chaumet, and G. W. Bryant, Astrophys. J. **607**, 873–878 (2004).
[147]M. A. Yurkin and M. Kahnert, J. Quant. Spectrosc. Radiat. Transfer **123**, 176–183 (2013).
[148]O. S. Vartia, P. Ylä-Oijala, J. Markkanen, S. Puupponen, A. Seppälä, A. Sihvola, and T. Ala-Nissila, J. Quant. Spectrosc. Radiat. Transfer **169**, 23–25 (2016).
[149]L. L. Jensen and L. Jensen, J. Phys. Chem. C **113**, 15182–15190 (2009).
[150]Y. He and T. Zeng, J. Phys. Chem. C **114**, 18023–18030 (2010).
[151]T. C. Preston and R. Signorell, Acc. Chem. Res. **45**, 1501–1510 (2012).
[152]T. Hayne and G. Weiser, Phys. Status Solidi B **123**, 271–280 (1984).
[153]S. Tavazzi, A. Borghesi, M. Campione, M. Laicini, S. Trabattoni, and P. Spearman, J. Chem. Phys. **120**, 7136–7140 (2004).
[154]C. C. Kim, J. W. Garland, H. Abad, and P. M. Raccah, Phys. Rev. B **45**, 11749–11767 (1992).
[155]E. E. Koch, A. Otto, and K. L. Kliewwer, Chem. Phys. **3**, 362–369 (1974).
[156]G. Weiser and S. Müller, Phys. Rev. B **65**, 045203 (2002).
[157]L. Raimondo, M. Laicini, S. Tavazzi, A. Borghesi, and P. Spearman, J. Chem. Phys. **122**, 064706 (2005).
[158]M. I. Alonso, M. Garriga, F. Alsina, and S. Piñol, Appl. Phys. Lett. **67**, 596–598 (1995).

[159]S. Tavazzi, M. Laicini, P. Lang, L. Raimondo, and P. Spearman, Org. Electron. **5**, 283–289 (2004).
[160]M. Dressel, B. Gompf, D. Faltermeier, A. K. Tripathi, J. Pflaum, and M. Schubert, Opt. Express **16**, 19770–19778 (2008).
[161]I. Vragovic, M. Schreiber, and R. Scholz, J. Lumin. **110**, 284–289 (2004).
[162]H. C. van de Hulst, *Light Scattering by Small Particles* (Dover Publications, Inc., New York, 2003).
[163]G. Weiser, Synth. Met. **139**, 719–722 (2003).
[164]H. Chatterjee and S. K. Ghosh, J. Phys. Chem. C **121**, 22310–22325 (2017).
[165]L. Yadgarov, C. L. Choi, A. Sedova, A. Cohen, R. Rosentsveig, O. Bar-Elli, D. Oron, H. Dai, and R. Tenne, ACS Nano **8**, 3575–3583 (2014).
[166]B. Champagne and D. M. Bishop, Adv. Chem. Phys. **126**, 41 (2003).
[167]C. Boukouvala and E. Ringe, J. Phys. Chem. C **123**, 25501–25508 (2019).
[168]M. Gluodenis and C. A. Foss, Jr., J. Phys. Chem. B **106**, 9484–9489 (2002).
[169]P. K. Jain, S. Eustis, and M. A. El-Sayed, J. Phys. Chem. B **110**, 18243–18253 (2006).
[170]R. Thomas, J. Kumar, J. George, M. Shanthil, G. N. Naidu, R. S. Swathi, and K. G. Thomas, J. Phys. Chem. Lett. **9**, 919–932 (2018).
[171]D. M. Solís, J. M. Taboada, F. Obelleiro, L. M. Liz-Marzán, and F. J. García de Abajo, ACS Nano **8**, 7559–7570 (2014).
[172]D. M. Solis, M. G. Araujo, L. Landesa, S. Garcia, J. M. Taboada, and F. Obelleiro, IEEE Photonics J. **7**, 4800709 (2015).
[173]J. Mc Donald, A. Golden, and S. G. Jennings, in Proceedings of the ISSS-7, 26–31 March 2005.